Solid Freeform Fabrication 2019: Proceedings of the 30th Annual International Solid Freeform Fabrication Symposium – An Additive Manufacturing Conference
Reviewed Paper

POWDER VARIATION AND MECHANICAL PROPERTIES FOR SLM 17-4 PH STAINLESS STEEL

Sean Dobson[*], Swathi Vunnam[*], Dana Frankel†, Chantal Sudbrack†, Thomas Starr[*]

[*] J. B. Speed School of Engineering, University of Louisville, Louisville, KY 40292
† QuesTek Innovation, Evanston, IL 60201

Abstract

Chemical composition and atomizing gas of powders may affect properties of 17-4 PH fabricated via selective laser melting (SLM) process. This study investigates 17-4 PH stainless steel powders with various atomizing gases and compositions within 17-4 PH specification range. Material characterization demonstrated differences in flowability between the powders, but all produced fully dense parts. The as-built phase composition varied widely, with samples from Ar-atomized powders ranging from a mostly martensitic grain structure to containing a significant amount of δ-ferrite depending on their composition, whereas samples from N_2 atomized powder contained largely austenite phase. After solutionizing and H900 hardening all Ar atomized powders produced homogeneous microstructure and improved mechanical properties meeting AMS 17-4 PH specification. The N_2 atomized powder produced a martensitic microstructure with retained austenite and only ultimate strength meeting AMS specification.

Keywords: selective laser melting, additive manufacturing, 17-4 PH stainless steel, microstructure, mechanical testing

Introduction

Additive manufacturing (AM) refers to a broad category of methods for turning computer aided design 3D models into a fabricated functional part. At its core, AM is the process of fabrication wherein material is added in a layer-by-layer fashion to form the part geometry. Modern AM methods appeared in the early 1950's with polymer material and has steadily grown. In the past decade AM has experienced rapid development as industry has begun to leverage its capabilities [1]. Metal AM has been at the forefront of research and development in the manufacturing field [2]. The ability to construct near net shape, fully functional metal components quickly in a cost-effective manner means limitless possibilities for many industries, particularly aerospace. Weight reducing brackets and assemblies printed as one large part are only the beginning for metal AM in aerospace [3]. Inside the category of metals AM there are several methods for fabrication, but the most widely used is powder bed fusion (PBF) [4]. This includes selective laser melting (SLM) and electron beam melting (EBM) and operates by mechanically spreading metal powder over the build followed by a laser or beam that melts the powder in the desired geometry. Following this the build volume drops and the process repeats until the part is complete.

A significant advantage for metal AM is that all the major metals used in traditional manufacturing are available for AM. For example, titanium alloys, inconel and variety of steels. One that is commonly used for its strong combination of properties and the focus of this study is 17-4 PH stainless steel. The precipitation hardening stainless steels are used in manufacturing for their heavily martensitic microstructures. When compared with austenitic steels, PH stainless steels

have a higher corrosion resistance and strength. This property combination applies up to temperatures of 315 °C meaning that this material is suitable for use in many applications [5]. For these reasons, 17-4 PH stainless steel is often used in AM research and there are numerous studies on the material.

For peak performance many metals, particularly precipitation hardening stainless steels, use thermal treatment to change the microstructure and improve mechanical properties. There are industry standards for these heat treatments which provide a certain set of properties dependent upon temperature, environment, and time of the treatment. Many past investigations examine thermal treatments and the resulting improved mechanical and microstructural properties of the materials [6-12]. In studies comparing 17-4 PH heat treatments it is found that the H900 treatment not only outperforms the solutionized material, but other hardening steps as well in achieving highest ultimate strength for tensile results [12]. This concurs with industry standard. Fabrication parameters also effect mechanical properties. In several studies it was found that build orientation results in anisotropy of mechanical properties with higher measured ultimate stresses in the horizontally fabricated specimens [8, 10, 13-15]. In one study it was found that higher treatment temperatures reduced anisotropy in specimens that were fabricated using SLM [8]. While this study does not involve 17-4 PH it demonstrates how thermal treatment can improve mechanical properties further specifically to AM.

To ensure that the parts fabricated are of the highest quality all steps of the process must be examined, especially materials. There are various methods for testing powder quality used in industry and research [16-20]. It is found in one study that particle characteristics have a strong influence over part density [18]. It was also noted that powder with a higher tap density resulted in greater densification. Another study determined that there should be more than one method used to characterize a powder, both static and dynamic testing [17].

Despite the attractive nature of AM, particularly SLM, and the use of materials such as 17-4 PH stainless steel, there remain certain obstacles that hinder the progression of this technology into mainstream manufacturing. A large obstacle currently is that there is not a full understanding of the process and how slight composition variation may affect part properties. It is currently unknown how vendor variation and powder manufacturing method will influence mechanical and microstructural behavior. This study seeks to characterize and understand the differences in powder and as-built properties between vendors and manufacturing methods. Following this, it is the goal of this study to effectively eliminate any variation through means of industry standard heat treatment and create uniform microstructural and mechanical properties for the 17-4 PH grade stainless steel AM materials and compare those to wrought specimens. Accomplishing this study will provide those necessary answers and help to further progress AM into the mainstream.

Materials and Methodology

Material

For this study the material used was 17-4 PH stainless steel. The 17-4 PH powder was received from three vendors with a particle size distribution of 15-45 μm. Two powders were procured from one manufacturer, each with a different gas atomizing manufacturing method, Ar and N_2. A

complete sample set stating anonymized vendor nomenclature and powder information can be found in table 1 below. The powders were selected due to their high frequency of use is SLM 17-4 PH processes.

Table 1. 17-4 PH stainless steel powder sample set basic variations.

Manufacturer	Powder State	Atomization Gas
Powder A	New	Ar
Powder B	New	Ar
Powder B	New	N_2
Powder C	New	Ar

There is some variation in chemical composition although all conformed within UNS S17400 specification range. The chemical compositions of the specimens were from the vendor provided datasheet and are given in Table 2.

Table 2. Composition of powders in wt %

powder	**Cr**	**Ni**	**Cr/Ni**	**Cu**	**N**	**Mo**	**Nb**
Powder A	16.12	4.15	3.88	3.21	0.006	-	0.2
Powder B Ar	16.70	4.29	3.89	4.49	0.031	0.05	0.27
Powder B N_2	15.50	4.55	3.41	4.50	0.099	.26	.24
Powder C	15.60	4.70	3.31	3.61	0.036	-	0.22
Wrought	15-17.5	3.0-5.0	-	0.0-5.0	-	0.0-0.5	0.0-0.45

Powder Testing

Powder flowability was tested using the Hausner ratio. The Hausner ratio is the ratio of tap to apparent density. Tap density is measured according to ASTM B527-06, in which powder is loaded into a graduated cylinder and tapped repeatedly allowing the powder to compact, removing void volumes. The volume is measured, and density is calculated from the total weight of the powder. Apparent density is determined by measuring the volume prior to tapping then calculated using the total weight of the powder. A powder is considered to have poor flowability with a Hausner ratio greater than 1.25 [23].

Particle size distribution was measured using light scattering method in accordance with ASTM B822-10. Utilizing the Microtrac S3500, ~10^{10} particles were measured then sectioned into 20 bands by diameter size. The test provides a particle size distribution of the powder sample by volume of powder for the measured diameter of the powder.

Internal powder porosity was measured and is the presence of the atomizing gas becoming entrapped within the powder particle upon powder fabrication. A small sample of each powder was mounted in epoxy resin and polished using a standard metallography preparation method.

Once polished, optical micrographs were taken of each powder in five separate fields. For each field an area fraction porosity was measured using an image analysis code written in MATLAB. The script converts each image to binary and traces each particle individually. The script then examines inside of each outlined powder particle and outlines each pore. Following this a calculation is made of total pore area to total area outlined and a percent porosity is output. A standard deviation is calculated from all measurements made.

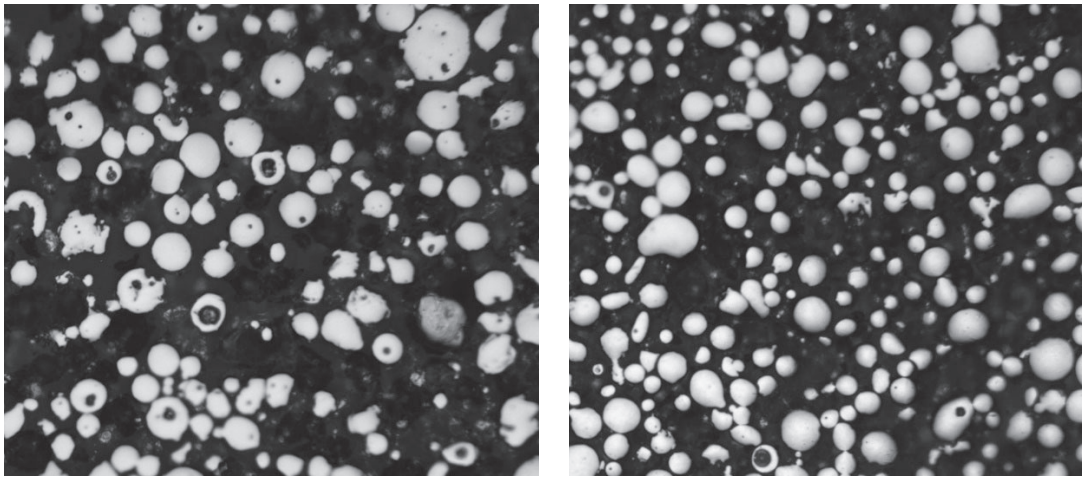

Figure 1. Polished sections of atomized powder show gas entrapped within some particles. The porosity is greater in Ar-atomized Powder B Ar (L) and N_2-atomized Powder B (R).

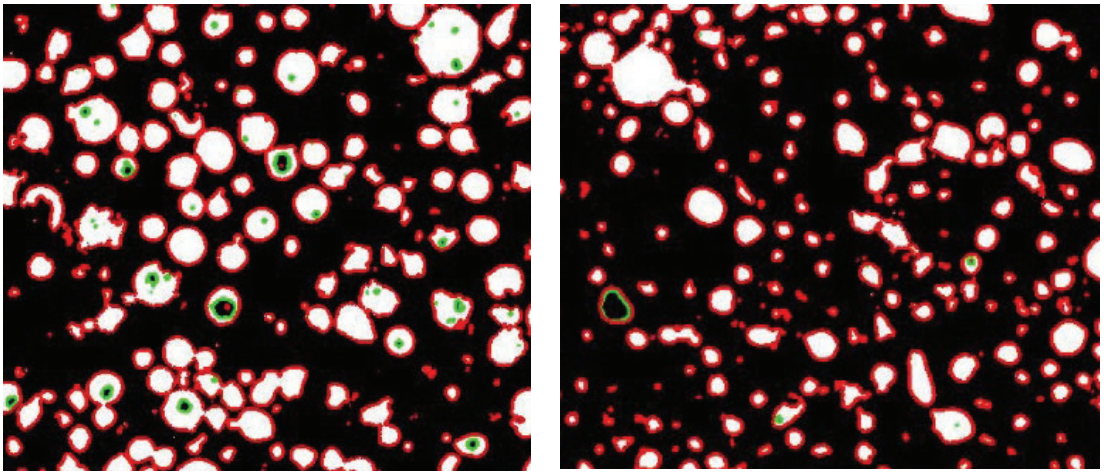

Figure 2. MATLAB script calculates internal porosity from micrograph images, Powder B Ar (L) and N_2 (R).

Sample Testing

A standard coupon set was fabricated for each powder using a commercial EOS M290 SLM machine. The exposure parameters were: power = 195 W, scan speed = 750 mm/s, hatch spacing = 0.100mm, and layer thickness = 0.040mm with standard contour/hatch scanning strategy and 67° scan rotation angle. A standard coupon set included microscopy coupons 9 x 10 x 11 mm cubes and larger rectangular bars, arranged in horizontal and vertical orientations for mechanical

properties. After thermal treatments, if applicable, specimens were wire EDMed into the shape of standard rectangular tensile bars.

All tensile specimens were in either of the two conditions: as-built/received or heat treated. The thermal treatment was a standard solutionizing and H900 hardening step. All AM samples not being tested in the as-built condition went through the solutionizing and H900 hardening step. The wrought material was already solutionized as-received and only hardened. The full heat treatment procedure can be found in Table 3 below.

Table 3. Heat treatment procedure.

Heat Treatment Step	Temperature (°C)	Treatment Time (hr.)	Cooling method
Solutionizing	1038	1	Air Quench
H900 Hardening	482	1	Air Quench

Microscopy coupons were sectioned in the XY (perpendicular to build direction) and Z (parallel to build direction) planes, mounted in epoxy resin and polished using standard metallography methods. The porosity of the as-built cubes was measured from optical micrographs using ImageJ software. Mean and standard deviation were calculated using five image fields. All samples were etched using Kalling's reagent # 2 to observe the microstructure, a mixture of copper chloride, hydrochloric acid, and ethanol.

Mechanical properties of the specimens were examined using monotonic tensile method according to ASTM E8-16. The tests were conducted on an Instron 50 kN load cell mechanical testing device (Model: 5569A). The test was conducted in a strain-controlled elongation to failure mode, with axial strain measured using a mechanical extensometer with gauge length of 12.5 mm. Three specimens of each condition were tested, and specimens met ASTM E8 standard design and dimensioning.

Results and Discussion

Table 4 contains results from the apparent and tap density measurements given as percentages of the true density of 17-4 PH stainless steel and the calculated Hausner ratio of tap to apparent density. Powders A, B N_2, and C all have similar flowability and are in the range of good flowability with a Hausner ratio ≤ 1.10. Powder B Ar has a lower level of flowability compared to the other powders but is still within the range of good flowability (<1.25 [23]). Figure 3 shows the distribution of particle size for the powders.

Table 4. Powder packing and flow behavior.

Material	Apparent Density (%)	Tap Density (%)	Hausner ratio
Powder A	55	58	1.06
Powder B Ar	49	59	1.21
Powder B N_2	58	63	1.09
Powder C	54	59	1.10

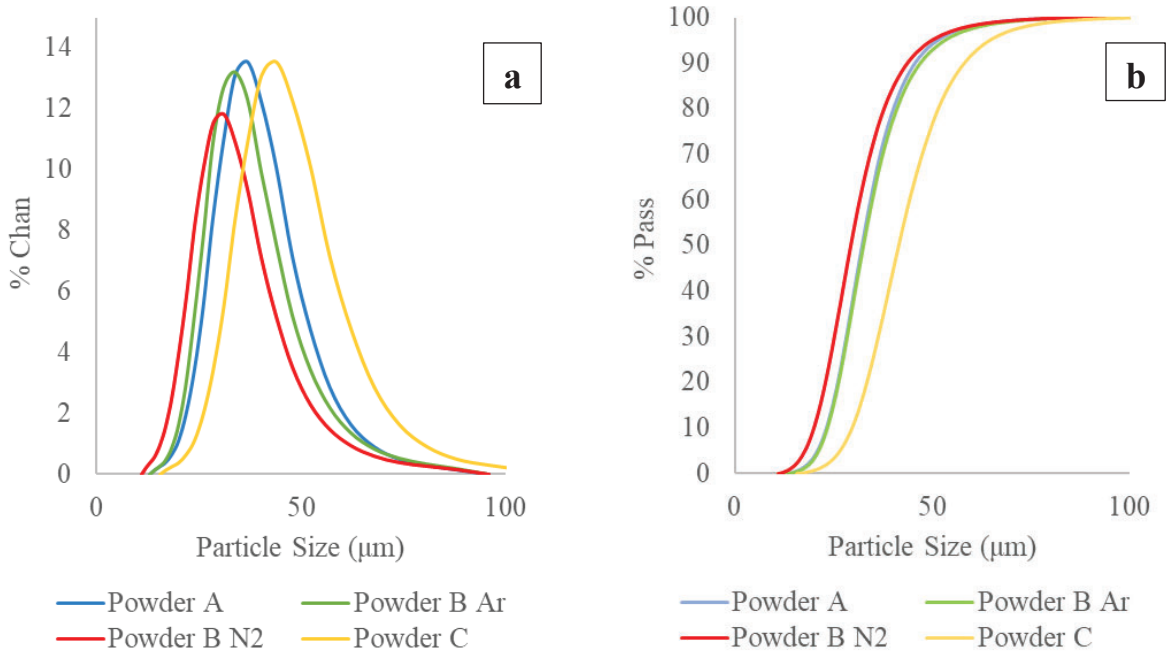

*Figure 3. Differential (**a**) and cumulative (**b**) particle size distribution of powders.*

Powder A and B Ar both have similar particle size distributions with a narrower particle size. Powder C has a similar narrow particle size; however, the distribution is shifted a small fraction towards a larger size distribution. Powder B N_2 has a wider distribution of particles, demonstrated by the shorter distribution peak. This is also reflected in the particle cumulation, Fig 3 (b). Powder B N_2 accumulates powder more rapidly with the cumulation line to the left of the other powders. Powder A and B Ar overlap completely and Powder C is significantly separated to the right again indicating a larger size distribution. There is no indication that particle size leads to any change in flowability. The three powders tested that were in the range of good flowability, Powders A, B N_2, and C, all had slight variations in their distribution and particle sizes and Powder B Ar, considered to have the poorest flowability, had a similar distribution to Powder A.

The porosity values measured are in Table 5 and the micrographs captured in Figure 4. The Powder B Ar had a significantly higher level of internal powder porosity than the other powder specimens,

despite large variation in porosity. The other three powders all had lower levels of internal powder porosity. There appears to be a correlation between internal powder porosity and flowability that could be a source of examination in the future to determine the cause. This is the possible explanation for powder B Ar having a substantially far poorer flowability than the other powders. Due to the higher level of internal powder porosity, there may be some deformation in morphology of the powder causing the difference in flowability.

Table 5. Porosity in coupons and in powder.

powder	% porosity		
	couponXY	**couponYZ**	**powder**
Powder B Ar	0.40 (.05)	0.44 (.06)	1.44 (.37)
Powder B N_2	0.03 (.01)	0.03 (.01)	0.17 (.10)
Powder C	0.10 (.01)	0.10 (.03)	0.29 (.27)
Powder A	0.05 (.01)	0.07 (.01)	0.24 (.23)

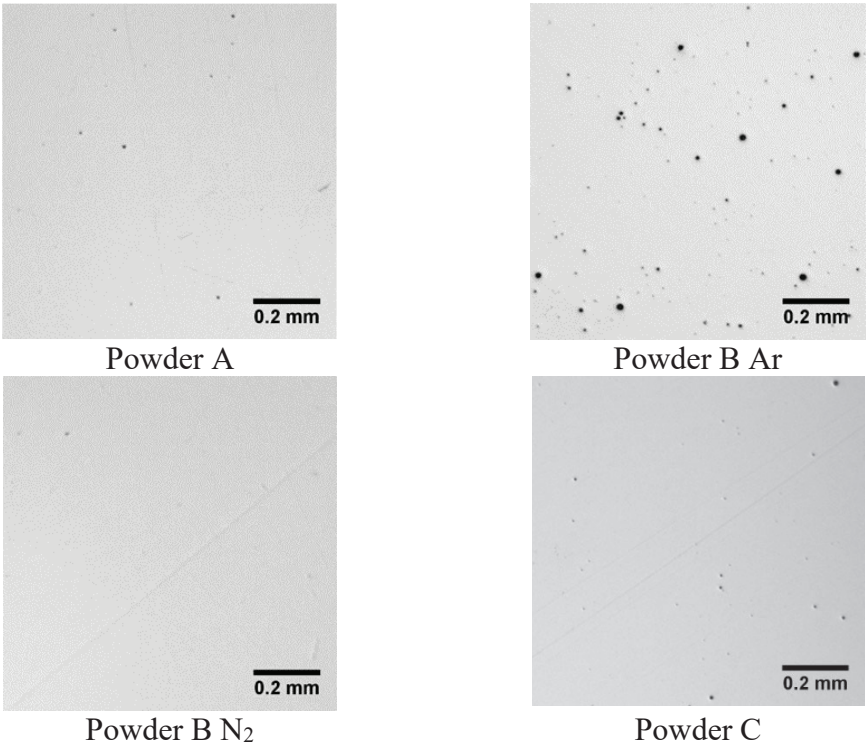

Figure 4. Optical micrographs of coupons from different powders.

The porosity measured in the XY and YZ planes are similar throughout all samples, that coupled with the low standard deviations suggests that the porosity was evenly distributed throughout each of the specimens. In the Powder B Ar coupon there was a significantly higher measured level of

porosity than the other powders, this is reflected in the micrographs in Fig 4. The two measured porosity levels, powder and coupon, demonstrate a strong positive correlation. This indicates that the cause of the coupon porosity is most likely due to the internal powder porosity. The fact that the measured powder porosity is higher than that of the coupon also suggests that much of the entrapped atomizing gas escapes. The morphology of the pores in powder and coupon, shown in Fig. 2 and 4 respectively, are similar in that they are spherical furthering the correlation. However, despite variation in powder characteristics all powders were able to fabricate fully dense specimens (>99.5% density) with the only measured porosity being spherical and attributed to internal powder porosity.

Figures 5 and 6 show tensile behavior and microstructure of the standard wrought material. After H900 hardening the yield stress increased by approximately 700 MPa after heat treatment and the ultimate strength increased by 400 MPa. The elongation to failure is typical for this material and the slight increase in elongation is indicative of the thermal treatment.

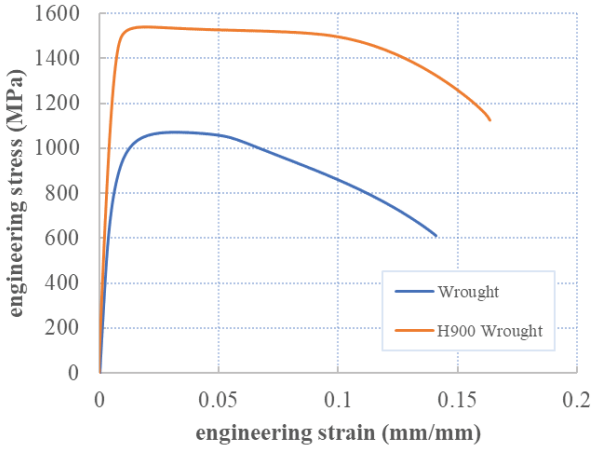

Figure 5. Wrought specimen as-received and H900 hardened tensile behavior

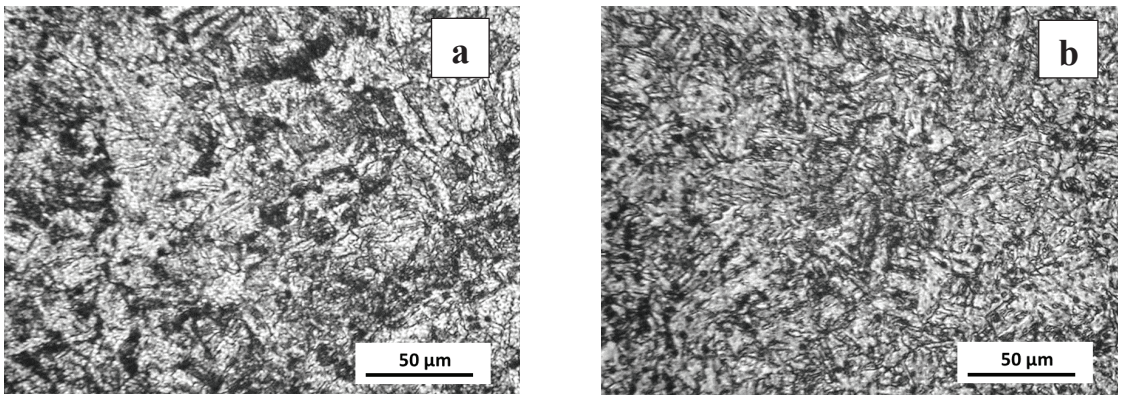

Figure 6. Wrought specimens as-received (**a**) and hardened (**b**) microstructure.

As expected for wrought 17-4 PH, a coarse-grain martensitic microstructure can be seen in Fig. 6 (a). The H900 thermally treated specimen in Fig. 6 (b) retains the martensitic grain structure but becomes more homogenous and refined with the aging process.

Fig. 7 is a full set of tests completed for the tensile specimens fabricated using SLM. All materials produced repeatable data in their tensile specimens. There was prevalent anisotropy in all materials with the ultimate strength of the horizontal being greater than the vertical direction. In Powder C the vertical specimens displayed a much smaller yield plateau, smaller elongation and lower ultimate strength.

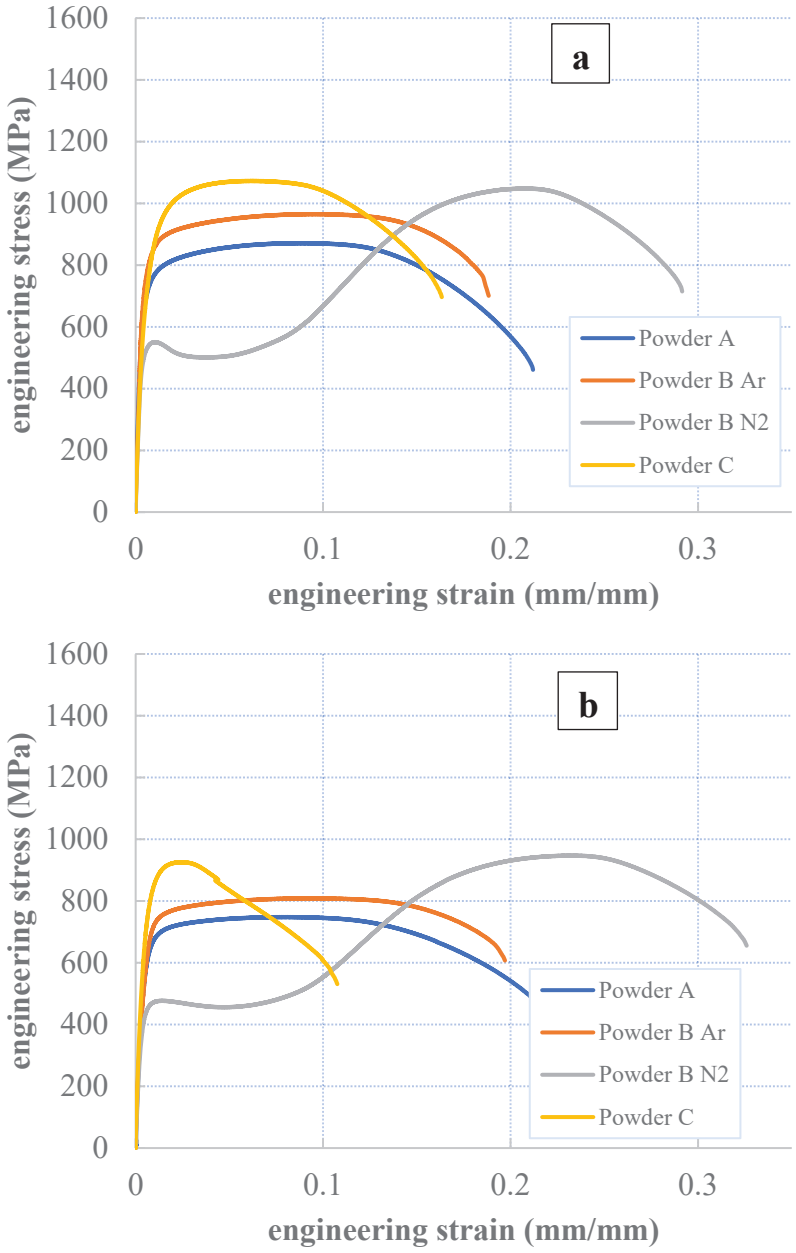

Figure 7. As-built specimen tensile data (**a**) horizontal and (**b**) vertical.

Powders A and B Ar had similar tensile performance with ultimate strengths of 900 MPa in the XY and 800 MPa in the Z. Powder B N_2 atomized tensile specimens performed completely different than the Ar atomized powders. There was a significant period of strain hardening at a low yielding strength in the initial necking region followed by another curve of increased strength. This strain hardening resulted in a significantly larger elongation to break for the Powder B N_2 specimens in addition to a high ultimate strength compared to Powder A and B Ar. This mechanical behavior indicates that the atomizing gas does influence part performance. Compared to the wrought solutionized (condition A) specimens all argon atomized powders behaved similarly, except the experienced anisotropy in the vertical Powder C specimens. Powder B N_2 reached both the same elongation and ultimate strength but behaved completely different. As for the H900 specimens, none of the powders performed as well as the hardened material in their as- built state. The microstructures for each as-built specimen is shown in Figure 8.

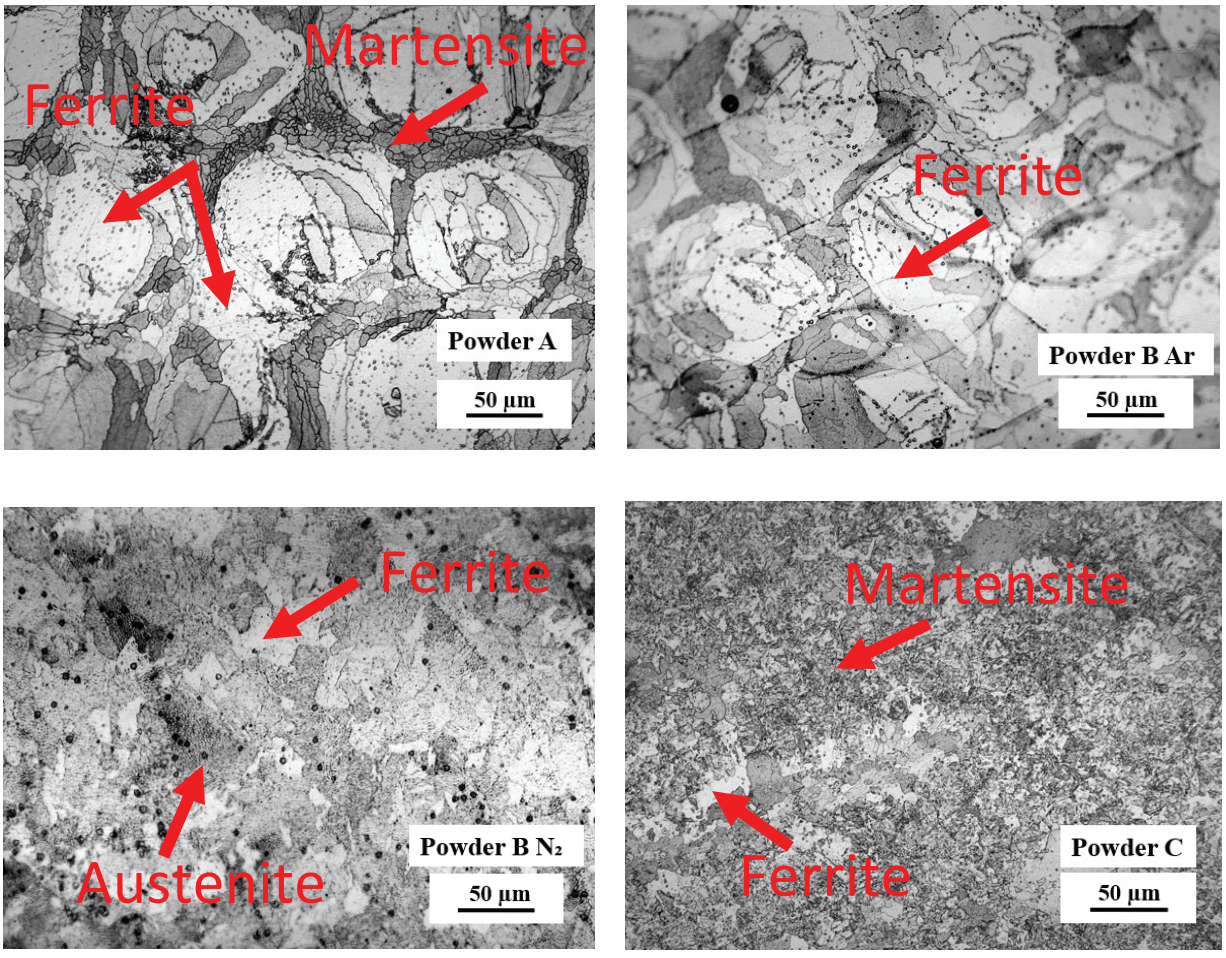

Figure 8. As-built microstructure of AM specimens (horizontal reference plane).

Despite using an identical parameter set with same grade stainless steel a range of differing microstructures were produced. Powder A and Powder B Ar produced similar microstructures with

larger ferritic grains (lighter contrast). Powder A also displays visible martensitic grain structures (darker) at the ferrite boundary. This similarity in microstructure is reflected in the similarity of mechanical properties. Powder B N_2 contains an inhomogeneous microstructure with large ferrite grains accompanied by a fine and equiaxed austenite grains. There is a significant amount of retained austenite present which is presumably the cause of the strain hardening, the dislocations were moved during plastic deformation upon which they became pinned and tangled. This reduced the mobility of the dislocation improving the strength and resulting in the material hardening effect. Finally, Powder C displays a microstructure that contains largely martensite with some retained δ ferrite [21]. The martensitic fine-grain structure improved mechanical strength as displayed in the tensile results. The as-built microstructure of SLM-processed 17-4 PH stainless steel is highly unpredictable. Before this material could be used in industry it would require a homogenized microstructure.

The differences in microstructure can be explained by chemical composition, Table 2, namely in the elements of chromium and nickel. All materials meet the specified chemical composition of wrought material, but the variation may be the cause of differences in mechanical and material properties. The chromium-nickel ratios of Powder A and Powder B Ar are extremely similar. This is again reflected in both the microstructure and mechanical performance. Powder C has chromium-nickel ratio that is much lower than the other specimens, but one that also overlaps with the specification of another grade of stainless steel, 15-5. This grade stainless steel also displays a heavily martensitic microstructure in the as-built condition [22]. The Powder B N_2 also has a lowed Cr/Ni ratio, but a much higher nitrogen and molybdenum content. This dissimilarity in microstructure between the same grade material is due to the variation in chemical composition within the specification boundary.

The complete set of tensile results for thermally treated specimens using the solutionizing and H900 hardening steps is provided in Figure 9. The solutionizing thermal step removed any anisotropy in the specimens that was noticed in the as-built state, the same result demonstrated in past studies. The hardening step improved mechanical strength properties greatly. However, elongation to failure was not improved during the H900 process in fact it was reduced. However, the reduced elongation does not inhibit these specimens from meeting full AMS specification. All Ar atomized specimens deformed between 10% – 12% before failure. The yield and ultimate strength were, however, greatly improved for each of these Ar atomized materials, comparable to the strength in the H900 state of the wrought. All Ar atomized specimens exceeded minimum specification for H900 processed 17-4 PH yield and ultimate strengths (1172 MPa and 1310 MPa, respectively). Powder B N_2 specimens' ultimate strength of the material was comparable with the wrought H900 specimen. However, the results display a far lower yield strength than the AMS specification. This yield strength is comparable to that of the material prior to strain hardening, implying that the material has not fully eliminated this effect. However, there was no noticeable hardening step, only a steady increase of stress and strain. In summary the solutionizing and H900 hardening step improved the AM argon atomized specimen yield and ultimate strength exceeding AMS strength specification, and all elongation met the standard. The yield strength of the N_2 atomized material do not meet standard due to a limitation in fabrication process.

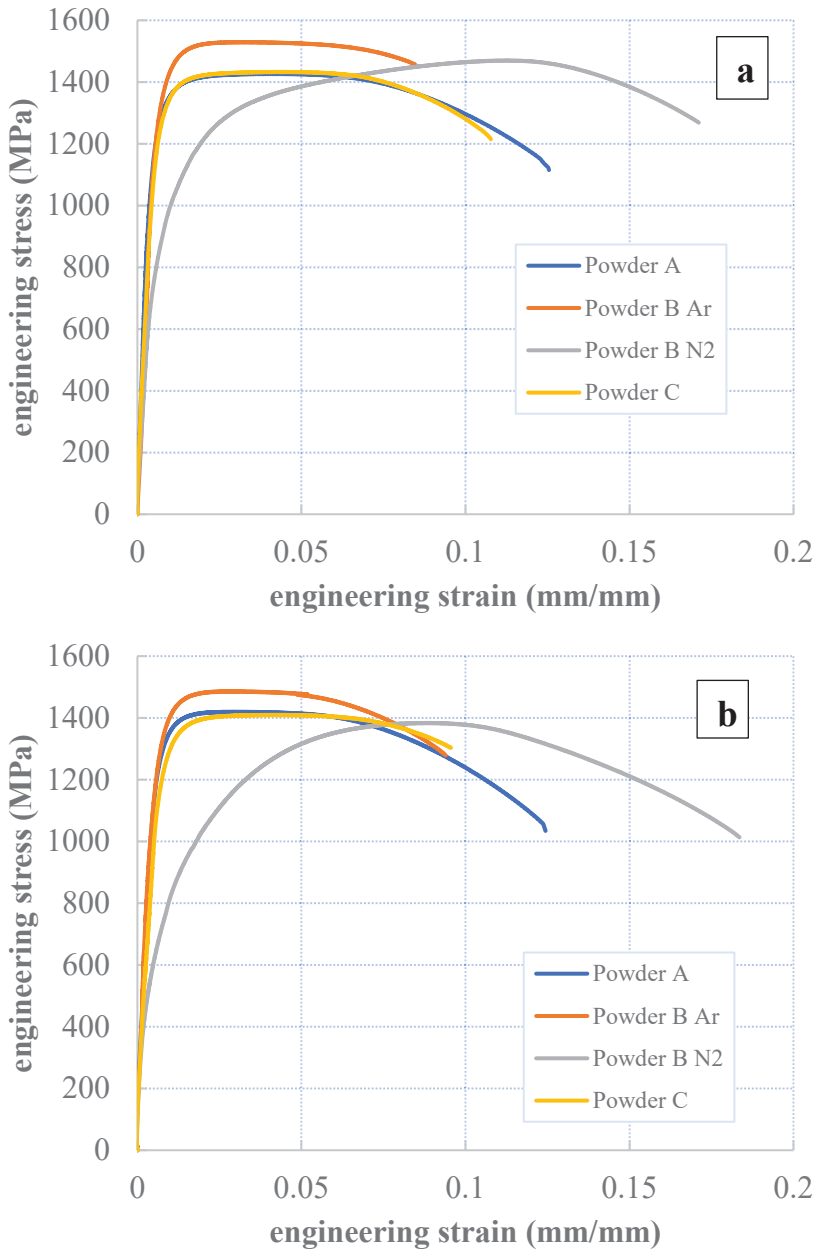

Figure 9. Solutionized and H900 hardened specimen tensile data (**a**) horizontal and (**b**) vertical.

The solutionized and hardened microstructures of the powder specimens are displayed in Fig. 10 below. The solutionizing step completely homogenized the microstructure into fine martensitic grains for the Ar atomized specimens allowing each specimen to be successfully hardened using H900 thermal treatment. This microstructure concurs with results from past studies that have performed a solutionizing step prior to hardening. The improved mechanical properties and similarity between that of the Ar atomized specimens can also be attributed to the thermal treatment microstructure. Powder B N2 has an inhomogeneous microstructure with brighter contrast in the middle of the samples and darker lathy microstructure around the brighter region as

shown in Fig. 11. The darker and brighter regions could be transformed martensite and retained austenite, respectively. From tensile data we can see the strain-hardening behavior of LPW N2 even after solutionizing and hardening indicating that there is a significant amount of retained austenite. However, further phase analysis is necessary to quantify the phase composition. Fig. 11 below demonstrates the mentioned darker lathy region and brightly contrasted regions found in the microstructure of Powder B N_2.

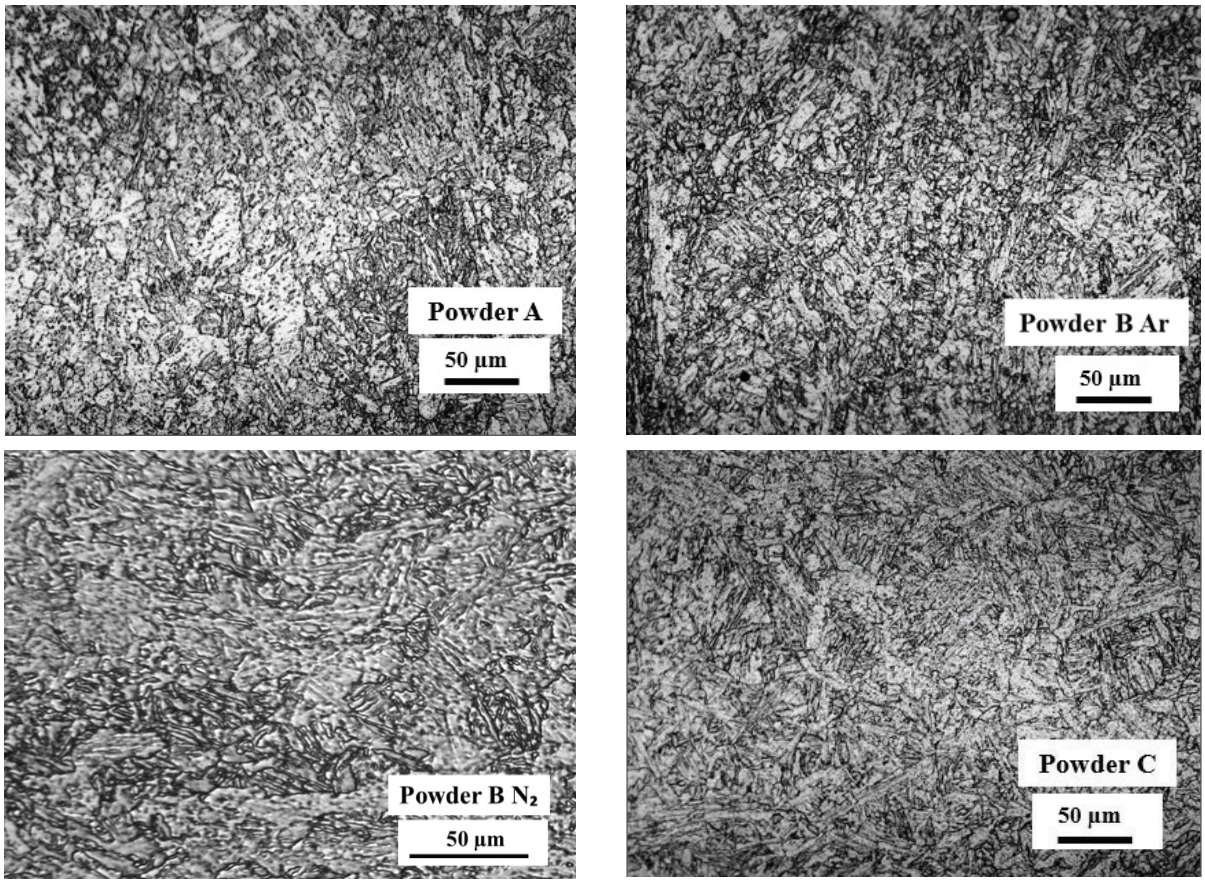

Figure 10. Solutionized and hardened microstructure of AM specimens.

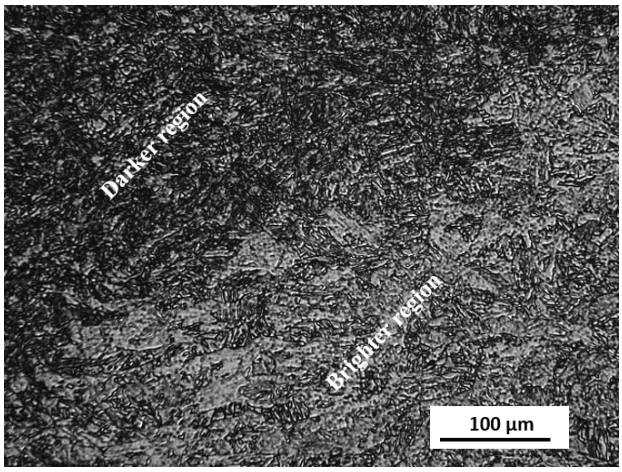

Figure 11. Microstructure of Powder B N_2.

Conclusion

In conclusion, there were measurable variations in powder flowability, particle size, and internal powder porosity. Despite these variations fully dense parts were fabricated. Internal powder porosity was shown to be the major cause of as-built porosity and is unavoidable despite an optimized parameter set. Chemical composition variation in same grade 17-4 PH stainless steel resulted in differing microstructures and mechanical properties. Atomizing gas also displayed an effect on microstructural and mechanical properties with N_2 atomizing gas producing an austenitic microstructure and strain hardening during tensile test. Ar atomizing gas produced both martensitic and δ-ferritic microstructures and displayed no strain hardening. Solutionizing thermal treatment successfully homogenized the microstructure and mechanical properties of each Ar atomized specimen, despite variations in chemical composition and powder characteristics. It improved the ultimate and yield strengths of all Ar atomized specimens, allowing them to meet AMS Specification, and the ultimate strength of the N_2 atomized specimen. The yield strength of the nitrogen atomized specimens was not improved through thermal treatment and retained some elements of its as-built strain hardening effects due to retained austenite post treatment. The solutionizing and thermal treatment removed anisotropic behavior that was present in the as-built specimens.

Acknowledgements

The U.S Naval Air Systems Command (NAVAIR) under contract number N68335-18-C-0020 funded the research work reported in this paper. We would like to acknowledge Mitch Gennocro from NAVAIR for serving as the technical mentor for this STTR project, and Kate Schneidau and Brittany Beaufait of the UofL Rapid Prototyping Center for fabricating specimens.

References

1. Zhai, Y., D.A. Lados, and J.L. LaGoy, *Additive Manufacturing: Making Imagination the Major Limitation.* JOM, 2014. **66**(5): p. 808-816.
2. Frazier, W.E., *Metal Additive Manufacturing: A Review.* Journal of Materials Engineering and Performance, 2014. **23**(6): p. 1917-1928.

3. Nickels, L., *AM and aerospace: an ideal combination.* Metal Powder Report, 2015. **70**(6): p. 300-303.
4. Duda, T. and L.V. Raghavan, *3D Metal Printing Technology.* IFAC-PapersOnLine, 2016. **49**(29): p. 103-110.
5. Yadollahi, A., et al., *Mechanical and Microstructural Properties of Selective Laser Melted 17-4 PH Stainless Steel*. 2015.
6. Cheruvathur, S., E.A. Lass, and C.E. Campbell, *Additive Manufacturing of 17-4 PH Stainless Steel: Post-processing Heat Treatment to Achieve Uniform Reproducible Microstructure.* JOM, 2016. **68**(3): p. 930-942.
7. Sun, Y., R.J. Hebert, and M. Aindow, *Effect of heat treatments on microstructural evolution of additively manufactured and wrought 17-4PH stainless steel.* Materials & Design, 2018. **156**: p. 429-440.
8. Alafaghani, A.a., A. Qattawi, and M.A.G. Castañón, *Effect of manufacturing parameters on the microstructure and mechanical properties of metal laser sintering parts of precipitate hardenable metals.* The International Journal of Advanced Manufacturing Technology, 2018. **99**(9): p. 2491-2507.
9. Sercombe, T., et al., *Heat treatment of Ti-6Al-7Nb components produced by selective laser melting.* Rapid Prototyping Journal, 2008. **14**(5): p. 300-304.
10. Mahmoudi, M., et al., *Mechanical properties and microstructural characterization of selective laser melted 17-4 PH stainless steel.* Rapid Prototyping Journal, 2017. **23**(2): p. 280-294.
11. Bhaduri, A.K., et al., *Optimized postweld heat treatment procedures for 17-4 PH stainless steels.* 1995.
12. Wu, J.H. and C.K. Lin, *Tensile and fatigue properties of 17-4 PH stainless steel at high temperatures.* Metallurgical and Materials Transactions a-Physical Metallurgy and Materials Science, 2002. **33**(6): p. 1715-1724.
13. Shrestha, R., et al. *Effect of Build Orientation on the Fatigue Behavior of Stainless Steel 316L Manufactured Via A Laser-Powder Bed Fusion Process*. in *27th Annual Solid Frefform Fabrication Symposium Proceedings*. 2016.
14. Yadollahi, A., et al., *Effects of building orientation and heat treatment on fatigue behavior of selective laser melted 17-4 PH stainless steel.* International Journal of Fatigue, 2017. **94**: p. 218-235.
15. Yadollahi, A., et al., *Data demonstrating the effects of build orientation and heat treatment on fatigue behavior of selective laser melted 17–4 PH stainless steel.* Data in Brief, 2016. **7**: p. 89-92.
16. Strondl, A., et al., *Characterization and Control of Powder Properties for Additive Manufacturing.* JOM, 2015. **67**(3): p. 549-554.
17. Krantz, M., H. Zhang, and J. Zhu, *Characterization of powder flow: Static and dynamic testing.* Powder Technology, 2009. **194**(3): p. 239-245.
18. Irrinki, H., et al., *Effects of particle characteristics on the microstructure and mechanical properties of 17-4 PH stainless steel fabricated by laser-powder bed fusion.* Powder Technology, 2018. **331**: p. 192-203.
19. Carrion, P.E., et al., *Powder Recycling Effects on the Tensile and Fatigue Behavior of Additively Manufactured Ti-6Al-4V Parts.* JOM, 2019. **71**(3): p. 963-973.

20. Yablokova, G., et al., *Rheological behavior of β-Ti and NiTi powders produced by atomization for SLM production of open porous orthopedic implants.* Powder Technology, 2015. **283**: p. 199-209.
21. S. Vunnam, A. Saboo, C. Sudbrack, T.L. Starr, *Effect of powder chemical composition on the as-built microstructure of 17-4 PH stainless steel processed by selective laser melting*, Additive Manufacturing (2019) 100876.
22. Spierings, A.B., T.L. Starr, and K. Wegener, *Fatigue performance of additive manufactured metallic parts.* Rapid Prototyping Journal. **19**(2): p. 88-94.
23. C. Conesa et al. (2004) "Characterization of Flow Properties of Powder Coatings Used in the Automotive Industry" Kona, Vol.22, pp 94-106.